ELSEVIER

Deep-Sea Research II 53 (2006) 60–76

DEEP-SEA RESEARCH
PART II

www.elsevier.com/locate/dsr2

Role of tides and mixing in the formation of an anticyclonic gyre in San Pedro Mártir Basin, Gulf of California

Efraín Mateos*, S.G. Marinone, M.F. Lavín

Departamento de Oceanografía Física, CICESE. Ensenada, Baja California, México

Received 2 February 2005; received in revised form 6 July 2005; accepted 7 July 2005

Abstract

A three-dimensional numerical model of the seasonal evolution of the hydrography and circulation of the Gulf of California predicts a quasi-permanent anticyclonic gyre in the central part of the gulf, over San Pedro Mártir Basin (SPMB), just South of the mid-gulf archipelago. A historical hydrographic data bank is used to search for evidence of the predicted gyre. Despite 363 useful profiles (in 15 cruises from 1939–1996), sampling in the area of interest only allowed climatological average distributions of temperature and salinity to be obtained, from which dynamic height and geostrophic currents were calculated. The average distributions of temperature, salinity and density all show a concave shape over SPMB, which translate into a dynamic height dome and therefore into and anticyclonic gyre. Vertical sections (across and along the gulf axis) of geostrophic velocity show that the gyre occupies most of the water column, which is 800 m deep in the center of SPMB. Experiments with the numerical model indicate that stratification is necessary, and that the tidal currents are responsible for the formation of the gyre; this occurs through nonlinear interactions (friction and advection) and vertical mixing, mechanisms that are enhanced in SPMB due to the proximity of the sills and channels of the midriff archipelago, where internal tides are generated.

Keywords: Tidal mixing; Tidal rectification; Anticyclonic gyre

1. Introduction

The Gulf of California is a marginal sea between mainland Mexico and the Baja California Peninsula (Fig. 1); it is approximately 150 km wide and 1100 km long. The general circulation of the gulf results from the tidal forcing and low-frequency motions at its opening, the forcing of the wind and atmospheric conditions at the sea–air interface and the nonlinear interaction of the flow with the topography. Seasonal circulation variability is due to the seasonal variability of these forcing agents (for a review, see Lavín and Marinone, 2003).

The tides in the gulf are in co-oscillation with the Pacific Ocean and the semidiurnal constituents are near resonance, with head amplitudes four times larger than those at the mouth of the gulf; e.g., the M2 tide has 36 cm of amplitude in the mouth and 150 cm in the head. The diurnal constituents are basically in phase in the entire gulf, and their amplitude increases toward the head by continuity (Lavín and Marinone, 2003).

*Corresponding author. Tel.: +52 646 175 0500; fax: +52 646 175 0568.
E-mail address: emateos@cicese.mx (E. Mateos).

0967-0645/$ - see front matter © 2006 Elsevier Ltd. All rights reserved.
doi:10.1016/j.dsr2.2005.07.010

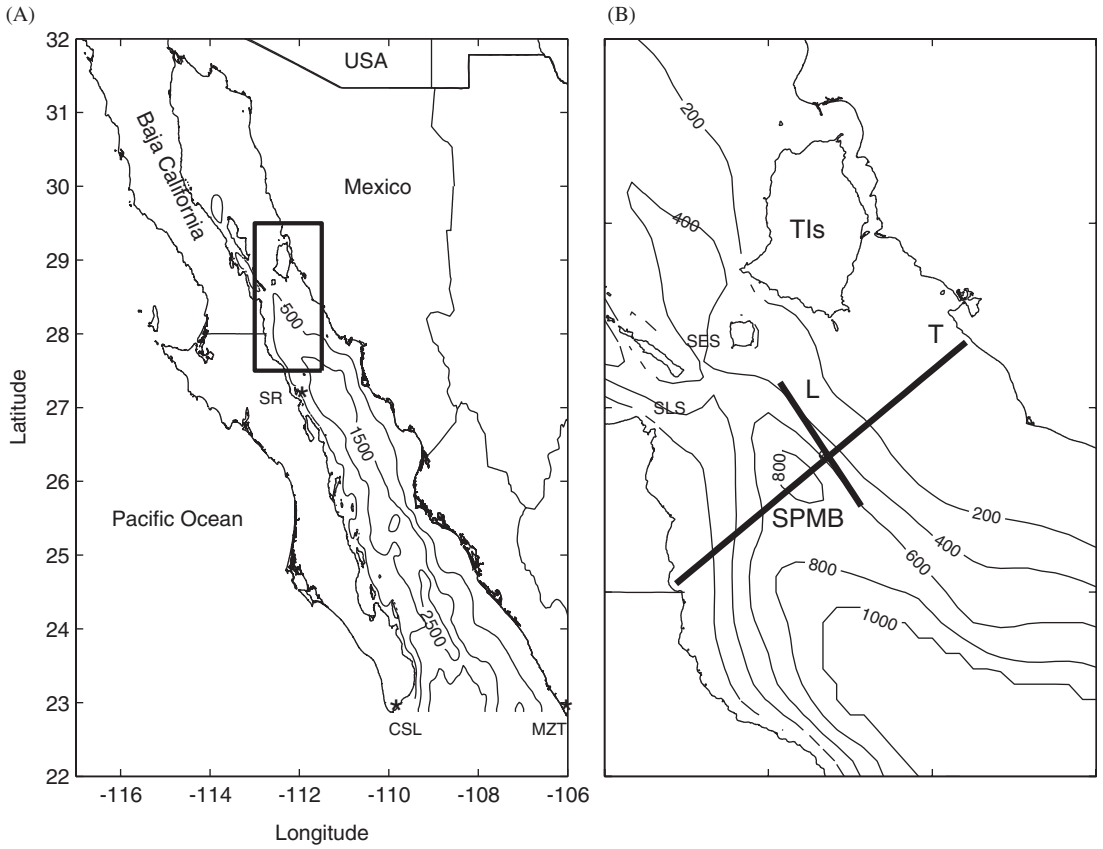

Fig. 1. Study area in the Gulf of California with bathymetric contours in meters. The square in (A) is expanded in (B) to show the San Pedro Mártir Basin (SPMB). The thick lines, labeled "T" and "L", are the transverse and longitudinal sections, respectively, for which salinity, temperature, density and geostrophic velocity sections are shown. In (A) CSL, MZT and SR with an asterisk mark the positions of Cabo San Lucas, Mazatlán and Santa Rosalía, respectively. In (B) SES, SLS and TIs stand for San Esteban sill, San Lorenzo sill and Tiburon Island, respectively.

The near-resonance of the semidiurnal tides, coupled with abrupt changes in bottom depth and cross-sectional area, causes very strong tidal currents in some places, especially in the shallow areas in the extreme North, and over the sills (~1.2 m/s over San Esteban Sill) and in channels of the midriff archipelago. This leads to dissipation of tidal energy in the northern region of the Gulf, as attested by the virtual amphidrome for the semidiurnal constituents inland of Santa Rosalía (SR in Fig. 1A) (Hendershott and Speranza, 1971; Filloux, 1973; Argote et al., 1995). The energy released by the barotropic tide in the northern region of the Gulf has very important physical and biological consequences; a fraction of this energy is used in vertical mixing.

Argote et al. (1995) used a vertically integrated numerical model to calculate the dissipation rate of semidiurnal tidal energy by bottom friction, and found an overall value of ~4 GW, most of it occurring in the northern region. They also found that in the shallow upper Gulf and in the island region (specifically over the sills) the dissipation rate is one order of magnitude stronger than elsewhere. Marinone and Lavín (2003) used a three-dimensional (3D) baroclinic model to show that internal mixing is also important in the channels and over the sills of the midriff archipelago. Physical evidence that mixing is occurring in those areas is provided by the well-established observation that the lowest sea-surface temperature (SST) in the Gulf occurs year-round precisely between the midriff islands, and especially over the sills. Argote et al. (1995) also showed that the observed stratification (measured by the potential energy) was weakened in the same areas. Paden et al. (1991) carried out a quantitative

analysis of satellite infra-red images of the Gulf, and concluded that the variability of the SST patterns is dominated by tidal mixing in the presence of surface heat flux and coastal upwelling; in the channels and sills, the semiannual and fortnightly variability of SST is strongly correlated with tidal mixing. Further observational evidence that tidal mixing around the midriff sills affects the thermohaline fields was provided by Simpson et al. (1994), who also suggested that this vertical mixing may have influence on the circulation and thermohaline structure over a wide area.

In addition to the extraction of tidal energy by bottom friction, and as a possible step toward dissipation and mixing, internal waves of various frequencies, from internal tides to high-frequency solitons are generated in the vicinity of the sills (Fu and Holt, 1984; Badan-Dangon et al., 1991; Filonov and Lavín, 2003). The internal solitons carry around 10% of the barotropic tide energy (Fu and Holt, 1984), while the energy of the semidiurnal internal tide is 40% of that of the barotropic tide (Filonov and Lavín, 2003).

In a previous study, Marinone (2003) showed a 3D numerical model of the Gulf of California, forced by the Pacific Ocean through specifying the sea level, the temperature and the salinity fields at the gulf entrance; at the sea surface, the wind and heat and freshwater fluxes are specified. The model reproduces the well-know general seasonal circulation of the northern gulf reported by Lavín et al. (1997). Additionally, Marinone (2003) predicts an anticyclonic gyre over the San Pedro Mártir Basin (SPMB, Fig. 1B), a small basin with maximum depths of ~850 m; the gyre does not show much seasonal variability. Marinone (2003) attributed the anticyclonic gyre formation over San Pedro Mártir Basin to tidal mixing, but no details were given.

Mesoscale gyres are common in the Gulf of California (Lavín et al., 1997; Pegau et al., 2002; Navarro-Olache et al., 2004), and for the southern part the observational evidence has been summarized by Figueroa et al. (2003); however, they did not look for a gyre over SPMB, because the analysis was made before it was predicted by Marinone (2003).

The objectives of this study are: (a) to use the numerical model to describe the characteristics of the gyre and to identify the agents and mechanisms responsible for its formation and maintenance and (b) to look for evidence of the existence of the gyre in a historical hydrographic data collection.

2. Methodology

2.1. Model

In order to find the forcing agents responsible for producing the anticyclonic gyre over SPMB, several runs with a 3D numerical baroclinic model were produced using combinations of different forcing agents: (a) the tidal forcing, (b) the Pacific forcing, (c) the winds, and (d) the heat and fresh-water fluxes. The run with all the forcing agents will be called the "Ref" run, the other runs are labeled with a *P*, *W*, and/or *T* indicating that the Pacific, wind or tidal forcing is included (see Table 1). The numerical model used in this study is the layerwise vertically integrated Hamburg shelf ocean model (HAMSOM). The governing equations of the model are a set of vertically averaged equations for each layer.

For momentum:

$$\partial/\partial t\, u = -h^{-1}\nabla_H\bullet(\mathbf{v}uh) - uH^{-1}\Delta(w) - fv - \rho_0^{-1}\,\partial/\partial x\, P + H^{-1}\Delta(\tau_x) + v\nabla_H^2 u,$$

and

$$\partial/\partial t\, v = -h^{-1}\Delta_H\bullet(\mathbf{v}vh) - vH^{-1}\Delta(w) + fu - \rho_0^{-1}\,\partial/\partial y\, P + H^{-1}\Delta(\tau_y) + v\Delta_H^2 v;$$

for continuity:

$$w_{z\mathrm{d}} = \partial/\partial x(uH) + \partial/\partial y(vH) + w_{z\mathrm{u}};$$

for temperature and salinity:

$$\partial/\partial t(T,S) = -\nabla_H\bullet[\mathbf{v}(T,S)] - h^{-1}\Delta[(T,S)w] + K_\mathrm{h}\,\nabla_H^2(T,S) + \partial/\partial z\, K_\mathrm{v}(T,S);$$

Table 1
Forcing agents included in the different simulations

	Forcing agents			
	Pacific	Wind	Tides	Heat and fresh water fluxes
Run name				
Ref	X	X	X	X
PWT	X	X	X	
PW	X	X		
PT	X		X	
WT		X	X	
P	X			
W		X		
T			X	

The nomenclature used in the run names is as follows: *P* for Pacific, *W* for winds, *T* for tides and Ref for all forcing mentioned before, plus heat and fresh-water fluxes.

the hydrostatic equation:

$$\partial/\partial z\, P = -\rho g;$$

the overall continuity equation:

$$\partial/\partial t\, \eta = -\nabla \cdot (\mathbf{V});$$

where $\mathbf{v} = (u,v)$ is the horizontal velocity, w is the vertical velocity, $\mathbf{V} = (U,V)$ are the transport for each layer, f is the local Coriolis parameter, $\rho = \rho(S,T,P)$ is the density field, (S, T, P) are salinity, temperature and pressure, g is the acceleration due to gravity, $P = (\eta - z)\rho_0 g + p(x,t)$ is the total pressure, p is the baroclinic pressure, h is the layer thickness which is equal to H, the nominal thickness, except in the first and last layers where it accommodates the surface elevation, η, and the topography, respectively. The operator $\Delta(\ldots)$ is the difference of $(\ldots)$ taken between the upper (zu) and lower (zd) surfaces of the layer.

The vertical stresses are $\tau = A_v(\partial/\partial z\, v)$ where A_v is the vertical eddy coefficient defined, following Kochergin (1987), as

$$A_v = \alpha|\partial/\partial z\, \mathbf{v}|/(1 + \beta Ri),$$

where Ri is the Richardson number, $\alpha = 10\,\mathrm{m}^2$ and $\beta = 10$. At the top and bottom, the surface and bottom stress boundary conditions are

$$\tau_s = C_{da}\, \mathbf{V}_w (U_w^2 + V_w^2)^{1/2},$$

and

$$\tau_b = C_{db}\, \mathbf{v} (u^2 + v^2)^{1/2},$$

respectively, where $\mathbf{V}_w = (U_w, V_w)$ is the wind velocity vector, C_{da} and C_{db} are drag coefficients for the air/water interface and for the sea bottom, respectively. Finally, K_h and K_v are the horizontal and vertical eddy diffusion coefficient for scalar quantities, which in the model are equal to v and A_v, the horizontal and vertical eddy viscosities. Note that the vertical eddy coefficients are function of space and time.

The model domain has a mesh size of $2.5' \times 2.5'$ (3.9×4.6 km). Twelve layers are used in the vertical, with nominal lower levels at 10, 20, 30, 60, 100, 150, 200, 250, 350, 600, 1000 and 4000 m. The number of layers depends on the local depth.

Several runs were performed forcing the model with the seven most important tidal constituents, viz. M2, S2, N2, K2, K1, O1 and P1, which account for more than 95% of the total tidal variance. The harmonic constants were estimated from several years of observations in Mazatlán, in the mainland side of the Gulf entrance, and in Cabo San Lucas, at the tip of the peninsula (see Fig. 1A). From these points, the sea-surface elevation was obtained at each time step and then interpolated along the open boundary. The bottom friction coefficient was varied in the different runs until the best agreement with observed tidal harmonics at several tidal stations around the gulf was obtained. The associated tidal currents, both barotropic and baroclinic, produced by the model have been compared with observations by Marinone and Lavín (2005), who find good overall agreement for the different tidal constituents. The best agreement is for the semidiurnal components, while the diurnal components are a little underestimated.

2.2. Hydrographic data

With the purpose of finding observational evidence of the anticyclonic gyre over SPMB, the Gulf of California hydrographic data bank was used. For this study area (Fig. 1), 15 cruises from 1939 to 1996 were extracted; producing a total of 363 casts (Table 2). Before 1980, temperature and salinity data were collected with reversing thermometers and sampling bottles, while from 1980 until 1996 CTDs were used; data every 10 db were obtained from all profiles.

Because there is poor spatial and temporal coverage in the historical hydrographic record, all

Table 2
Cruises used to obtain hydrographical data

Cruise	Month	Year	Casts	Used casts	Vessel
1	March	1939	47	4/5	*E.W. Scripps*
2	February	1957	53	5/6	*Horizon*
3	November	1961	40	9/11	*H.M. Smith*
4	November	1972	97	6/11	
5	March	1983	103	11/16	*El Puma*
6	October	1983	44	6/14	
7	March	1984	119	13/19	*New Horizon*
8	May	1984	172	31/31	*New Horizon*
9	November	1984	97	15/23	*New Horizon*
10	March	1985	77	10/21	
11	November	1985	147	43/74	*El Puma*
12	January	1990	125	66/73	*El Puma*
13	February	1990	143	13/22	
14	June	1995	132	12/19	*Francisco Ulloa*
15	August	1996	65	9/18	*Francisco Ulloa*
Total			1461	253/363	

The first figure in used casts indicates the number of casts that reach at least 250 db.

available data had to be combined and interpolated to form a single climatological average map. Of the 363 casts available, only 253 could be used to calculate an average dynamic topography map using 250 db as a reference level. Geopotential anomalies were calculated according to Pond and Pickard (1983), from salinity and temperature profiles, and then objectively interpolated in a regular grid with a resolution of 7 km. The correlation function used was a Gaussian, exp$(-\lambda^2/L^2)$ with $\lambda = 40$ km and $L = 200$ km. As will be shown below, the data were sufficient to test for the presence of the quasi-permanent gyre.

Vertical profiles of T, S and ρ were explored with the purpose of identifying structures revealing the gyre over SPM Basin. Longitudinal and transverse sections ("L" and "T" sections, respectively, Fig. 1B) of the variables mentioned above were made. These profiles were obtained from the objective interpolation of all the 363 casts. Geostrophic velocity fields also were obtained from the interpolated T and S fields. The geopotential anomalies were estimated using the maximum common depth of each pair of casts as reference level, following the traditional dynamic method (Pond and Pickard, 1983). For the across-gulf section ("T" section), an estimate of the absolute velocity was made, by requiring mass conservation in the section, following Fomin (1984) and Marinone and Ripa (1988).

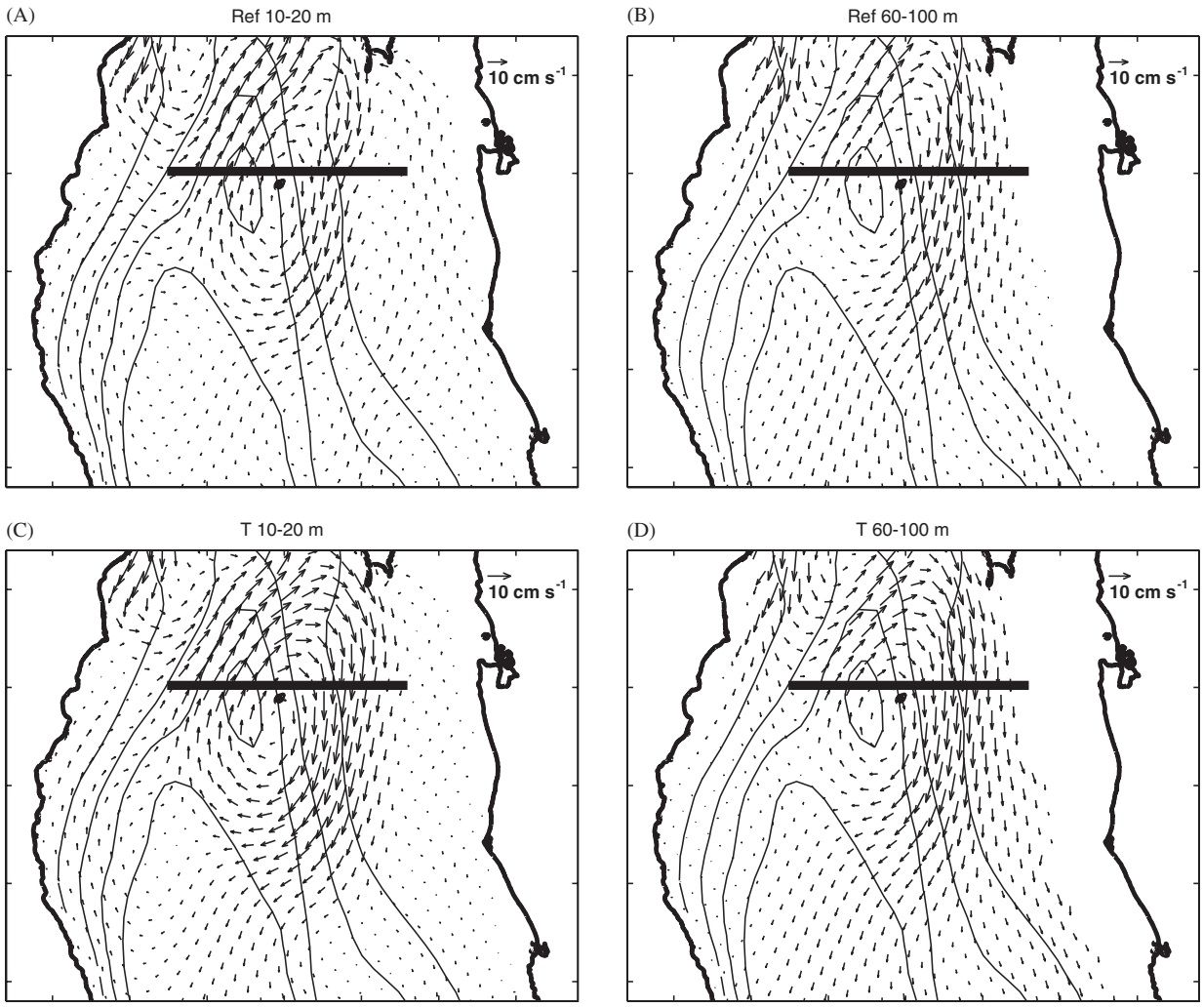

Fig. 2. Annual mean of the Ref (top) and T (bottom) simulations on a surface (10–20 m) and an intermediate (60–100 m) layer. The thick lines correspond to that part of the transverse section where the gyre is located and for which vertical sections are shown below.

3. Results

3.1. Model circulation

3.1.1. Climatological structure

The annual average current distribution for the 10–20 m and 60–100 m layers produced by the Ref simulation (Figs. 2(A) and (B)) show a well-defined anticyclonic gyre over SPMB, with speeds ~12 cm/s in the 10–20 m layer. The distribution of the speed normal to the "T" cross-section (Fig. 3A) show that the gyre occupies most of the water column; the outflow branch of the gyre is over the continental shelf on the mainland side (maximum speed 9 cm/s) and is ~350 m deep, while the inflow takes place in the deep central region of the basin (maximum speed 6 cm/s) and seems to be as deep as the basin (although the speed is only ~2 cm/s from ~100 m depth to the bottom). Over the peninsular continental shelf, outflow is present in the upper 250 m, which is also apparent in the surface distribution velocity field (Fig. 2 top). The equivalent results for the PWT run were almost identical to Fig. 3A, and therefore are not shown.

The annual-average distributions of velocity produced by the *T* simulation (only tidal forcing) are almost identical to those of the Ref run, both in the horizontal (Fig. 2) and in the vertical (Figs. 3(A) and (B)); they contain the gyre over SPMB and the coastal flow over the peninsular continental shelf. All the runs that included tidal forcing (Table 1) produced horizontal and vertical distributions of velocity (not shown) that are very similar to those of the *T* or Ref runs (Figs. 3(A) and (B)).

The runs in which only the wind or Pacific forcing (*W* and *P* simulations) are used do not produce the anticyclonic gyre, therefore their horizontal velocity distributions are not shown. The speeds normal to the "T" section for these two runs (Figs. 3(C) and (D)) are much smaller (<1 cm/s) than those in the Ref run (Fig. 3A).

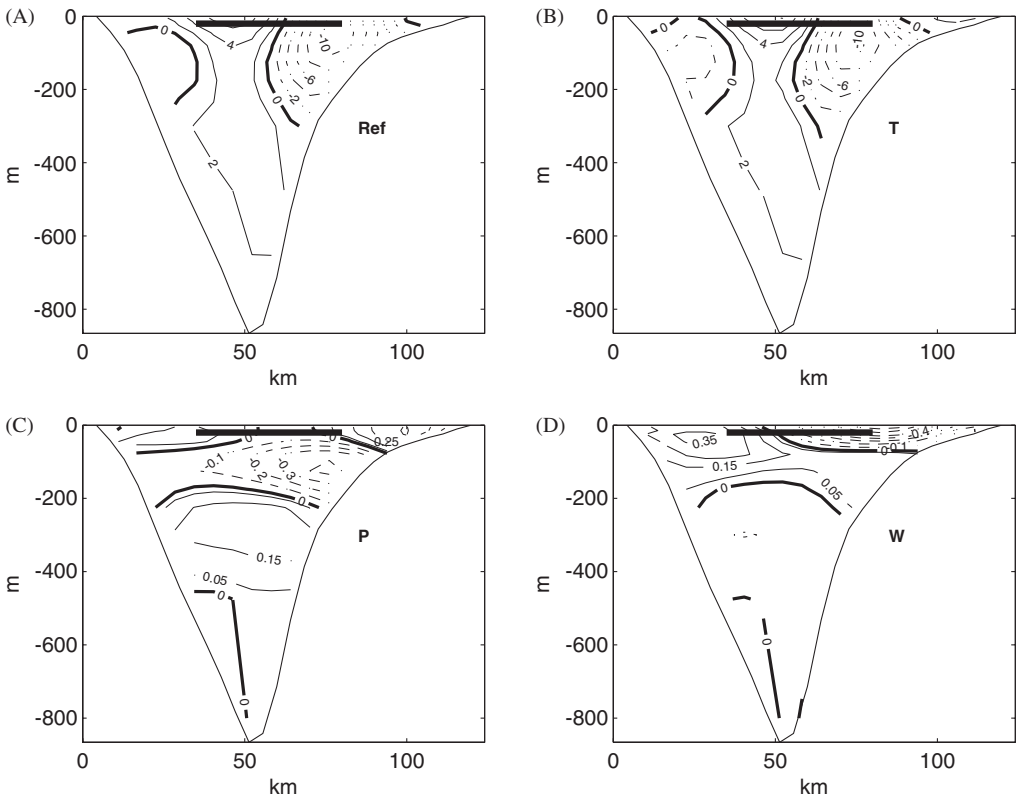

Fig. 3. Transverse cross-section (looking up-gulf, see Fig. 1) of the annual mean along gulf velocity (cm/s) for the (A) Ref, (B) *T*, (C) *P*, and (D) *W* simulations. The horizontal thick line shows the position of the gyre (see Fig. 2). Negative and positive velocities are to the South and North, respectively. The section is viewed from the South, so that the left side corresponds to the West coast, i.e., the Baja California peninsula.

The results above mean that tidal forcing is responsible for the generation of the anticyclonic gyre over SPMB. The possibility that the nonlinear interaction of the tidal currents with the bathymetry (tidal rectification) was causing the gyre was investigated by removing the temperature and salinity structure (homogeneous condition) and running the model with only tidal forcing; the anticyclonic gyre was not produced. Thus, it can be concluded that stratification and tidal forcing both play an important role in the formation and permanence of the anticyclonic gyre. It is proposed that this occurs because of vertical mixing, through the generation and breaking of internal tides, as discussed below.

In addition to the annual-average velocity structure, the monthly averages also were analyzed. For the *T* run, the gyre over SPMB is present in every month. In the Ref run, however, the gyre is hidden or modified in some layers, mainly in the Summer. From the analysis of the several combined runs shown in Table 1, it is concluded that although the Pacific and wind forcings are not sufficiently strong to affect the gyre on an annual mean, they can inhibit or modify the gyre in the months when they are most intense (e.g. in August for the wind).

3.1.2. M2 simulation from rest, and evidence of mixing

It was found that the gyre was formed very soon after the initiation of the runs that contained tidal forcing. In order to investigate this feature, a simulation from rest under stratified conditions

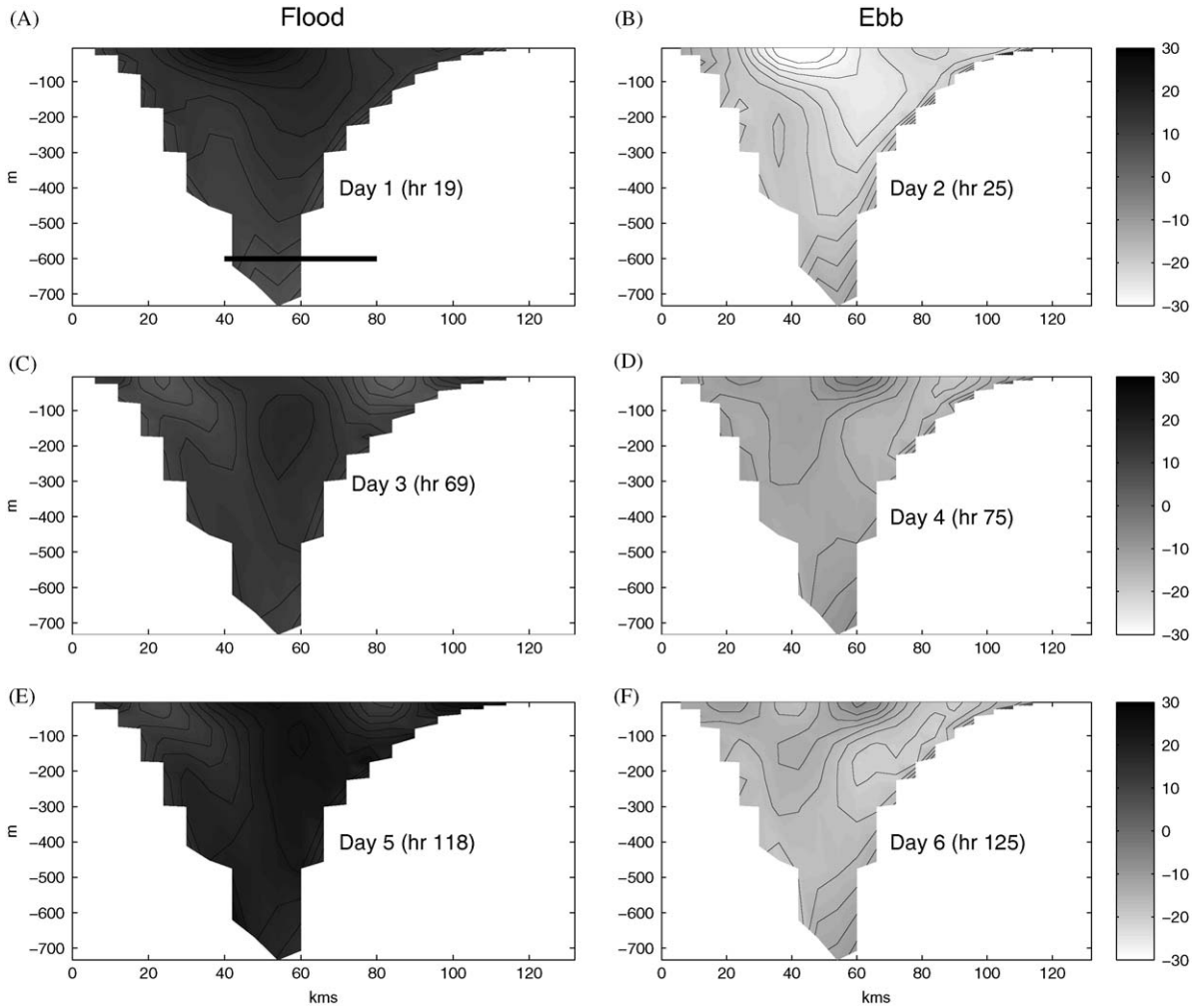

Fig. 4. Evolution of the velocity field across section "T"(looking up-gulf, see Fig. 1) with only the M2 tidal forcing during flood and ebb for: (A) and (B) second day, (C) and (D) fourth day, (E) and (F) sixth day. The horizontal thick line in (A) shows the position of the gyre.

with only the M2 tidal constituent was made (the M2 run). Fig. 4 shows the instantaneous velocity field on the flood and ebb on the indicated days, which correspond to the second, sixth and tenth tidal cycle of this run. At the beginning of the simulation (first tidal cycle, not shown) the flow basically comes in and out as a barotropic flow. By the second day, vertical and horizontal shears are present. During the flood (Figs. 4(A), (C), and (E)) the isolines of velocity acquire an almost vertical structure in the central zone, producing strong lateral shear even in the deep area.

The very strong vertical shear in the basin's central zone (Fig. 4A) suggests that turbulent mixing may be generated in that zone. Evidence for mixing is present in the evolution of the temperature field in the "T" section at days 2, 4, 6 and 60 of the M2 run (Fig. 5): (a) the isotherms above 10 °C acquire a concave shape by the sixth day of the run (Fig. 4F) and (b) by day 60 vertical stratification is clearly reduced, as indicated by the vertical temperature gradient. We propose that these features are consequences of tidal mixing, as discussed below.

3.2. Observations

The distribution of dynamic height (relative to 250 m) was obtained for every cruise (not shown), and it was found that the gyre was not defined in most of the individual cruises, mainly because the sampling was not adequate: either the station separation was too large or the sampled area was too small, or there were very few stations in the area. It was not even possible to construct a seasonal evolution of the dynamic height. Since the gyre was predicted to be present in the annual average, climatological means were constructed separately with data from the cruises that did or did not show some evidence of the gyre; both

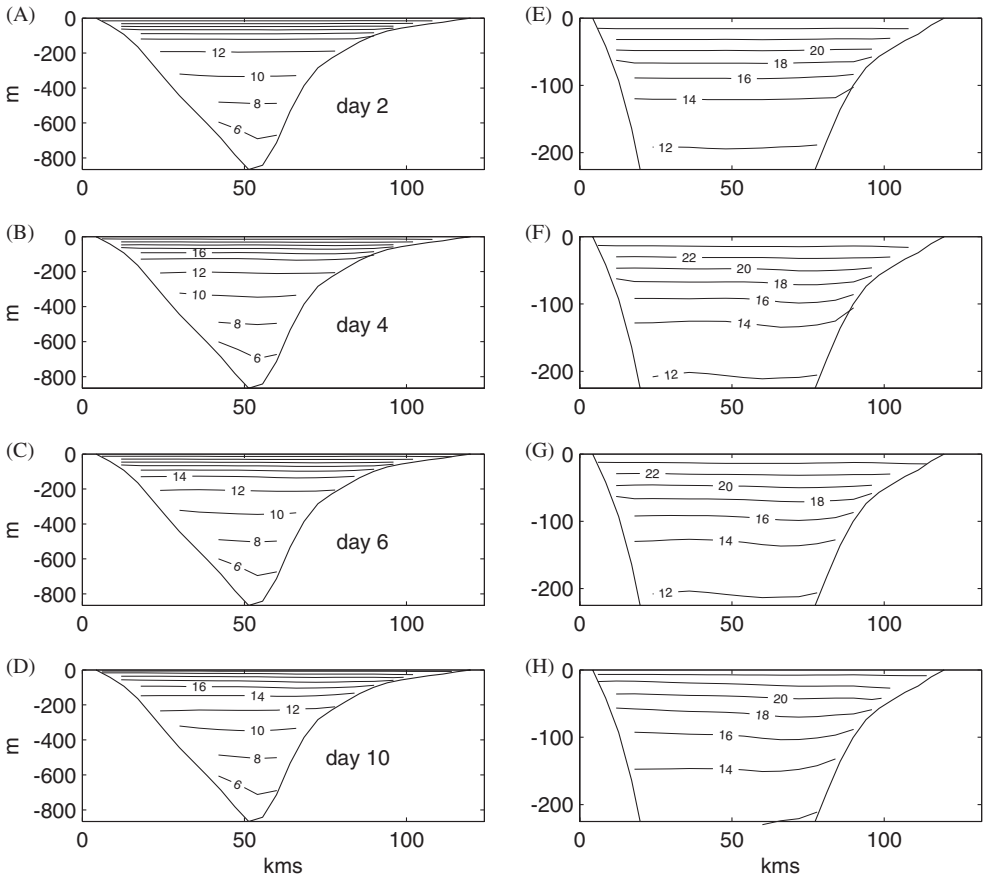

Fig. 5. Daily mean temperature field for the M2 run on section "T" (looking up-gulf), for days (A) 2, (B) 4, (C) 6, and (D) 60. The right panels, (E), (F), (G), and (H) correspond to the first 225 m of the corresponding left panels ((A), (B), (C), and (D)).

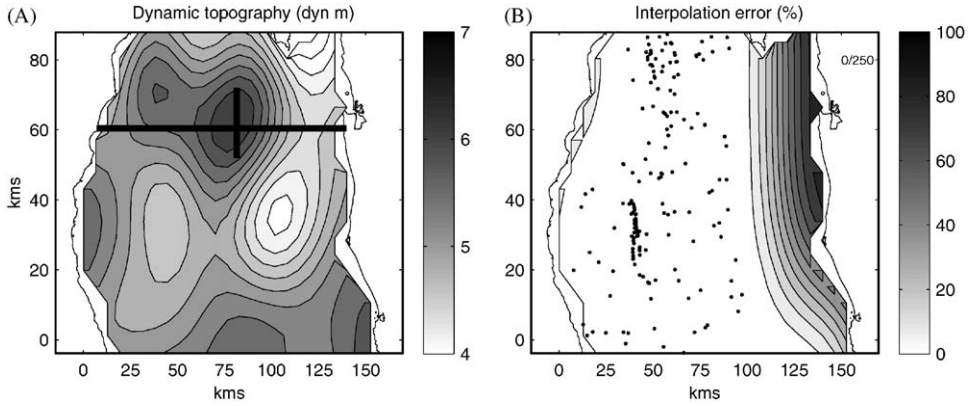

Fig. 6. (A) Dynamic topography in Dyn m (relative to 250 db) using all hydrographic data available. (B) Error percent of the interpolation method. Dots indicate the position of the individual cast. The thick lines in (A) mark the "L" and "T" sections for which vertical distributions are shown below.

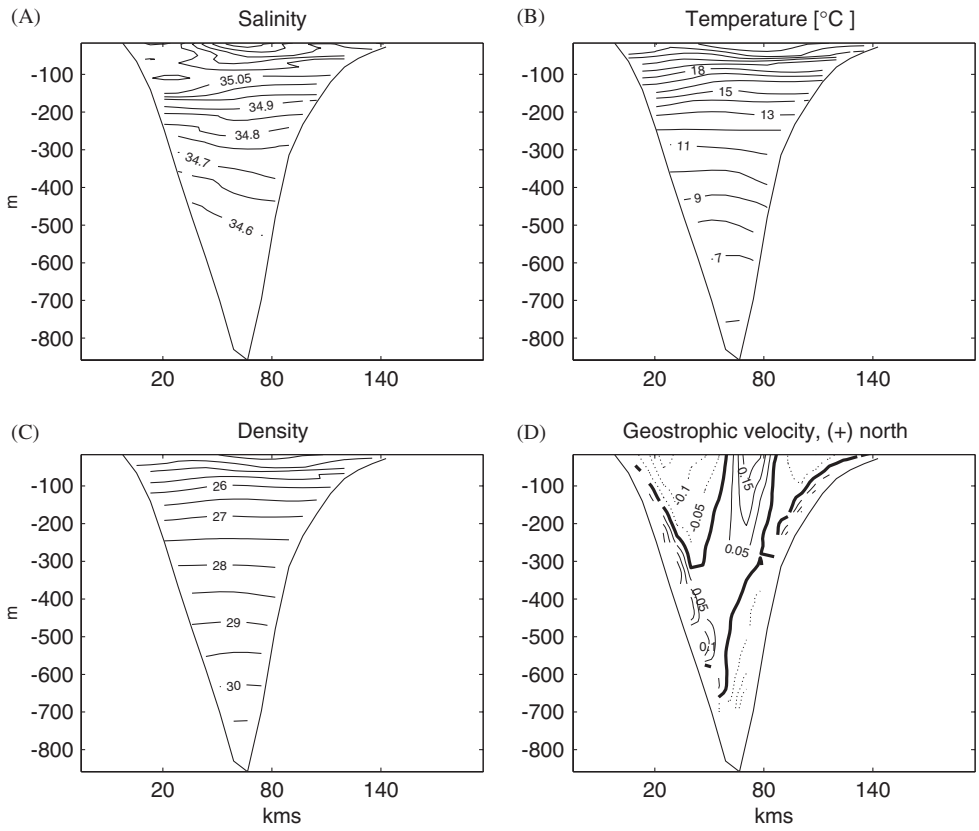

Fig. 7. (A) Salinity, (B) temperature (°C), (C) density (σ units), and (D) geostrophic velocity (m/s) across "T" section in the SPMB (looking up-gulf).

climatologies produced the gyre. Therefore a climatology of dynamic height with all the data was constructed; it shows (Fig. 6) quite definitely the anticyclonic gyre over the SPMB, thus proving the model prediction. The rms error is less than 2% in the area occupied by the gyre.

The average distributions of salinity, temperature, density and geostrophic velocity on the "T"

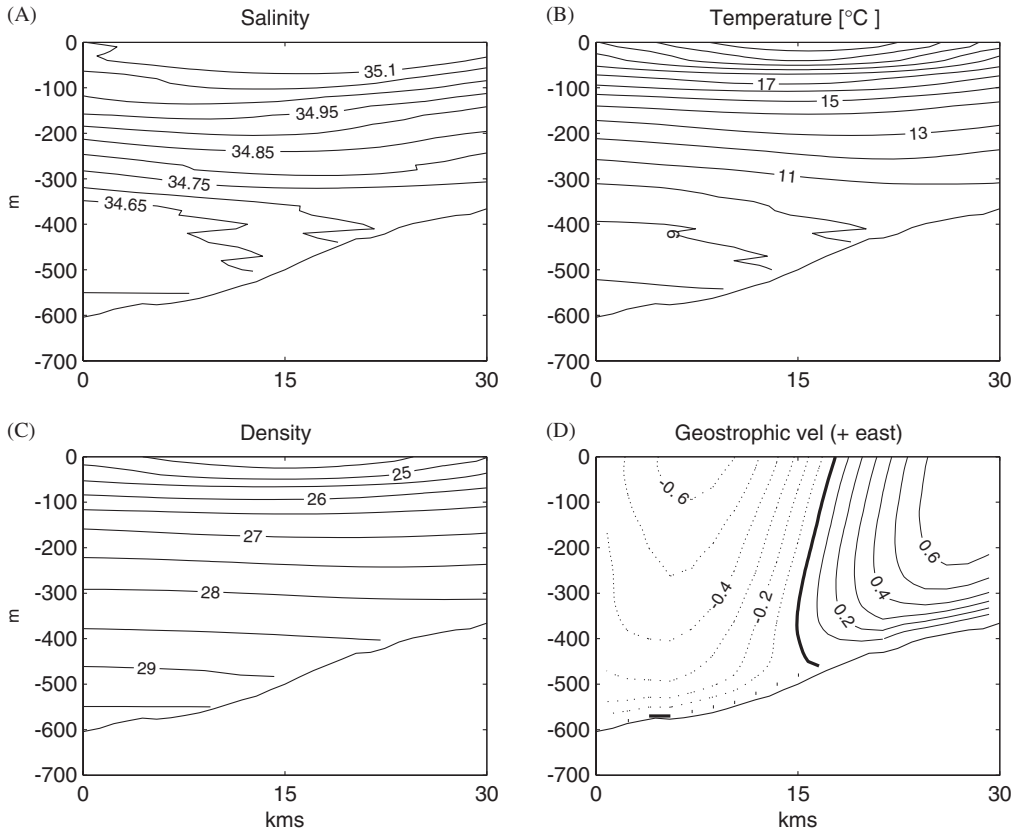

Fig. 8. (A) Salinity, (B) temperature (°C), (C) density (σ units), and (D) geostrophic velocity (m/s) across section "L" (looking West) in the SPMB. Positive velocities point toward the mainland (approximately NW).

section are shown in Fig. 7. The temperature and density distributions show some doming in the layers below 400 m, and upward concavity of the isolines above that depth. Above ~100 m, the isotherms and isopycnals show a strong downward (upward) tilt toward the mainland (peninsula) side. Surface temperature and salinity in the peninsula side are ~19 °C and 35.25, while in the mainland side they are ~23 °C and 35.3. The density field is similar to the temperature field, although the vertical gradients are weaker in the top layers due to the opposing influence of salinity decreasing downward. The velocity field (Fig. 7D) shows, in the upper 300 m, two cores of southward flow immersed in mostly northward flow; the velocities are maximum at the surface (~0.1 m/s). The two southward cores flank a northward core in the center of the basin. The gyre in SPBM is formed by the positive core and the eastern southward one. The gyre spans a large proportion of the water column. There is also inward flow close to the bottom on both shelves and platforms, except in the eastern side where outward flow occurs between 300 and 800 m.

The vertical distribution of salinity and temperature on the "L" section (Figs. 8(A) and (B)), show a concave structure of the isohalines and isotherms, even clearer than for the "T" section, reaching to 300 m. This concavity of the isolines is a product of a general downward tilt to the North, and a fanning out in the vertical over the shallower area. The corresponding isopycnals (Fig. 8C) display the same general shape as the isotherms and the isohalines, although below ~300 db they are less tilted. The geostrophic velocity in this section (Fig. 8D) shows a very clear anticyclonic gyre: westward flow in the South of the basin and eastward flow in the North. Both branches have a maximum velocity ~0.6 m/s, which is several times faster than in the "T" section (0.1 m/s). The gyre occupies almost all the water column.

4. Discussion

The observations support the existence, in the long-term mean, of the SPMB gyre predicted by the numerical model. However, more appropriate data are needed to resolve its features and variability; the position and dimensions of the gyre are such that a series of short cruises may suffice. Meanwhile, the numerical model results can be used to improve our understanding of the gyre and to areas where further studies are needed.

Observational and model results both indicate that the anticyclonic gyre over SPMB is, at least in part, a consequence of the vertical spreading of the isopycnals in the vicinity of the northern limit of the southern gulf. This area has long been known to be characterized by strong vertical mixing, associated to the strengthening of the tidal currents as the bathymetry rises to the archipelago (Badan-Dangon et al., 1985; Paden et al., 1991; Simpson et al., 1994; Argote et al., 1995). The vertical spreading of isotherms as the shallow area is approached from the South was described by Navarro-Olache et al. (2004), who also ascribed it to vertical mixing.

By weakening or breaking down stratification, tidal mixing changes the density field, sometimes to the extent of producing thermal fronts, and consequently residual currents parallel to the front (Simpson, 1981; Takeoka et al., 1997). The way in which spatially varying tidal mixing leads to currents and gyres has been well studied in the context of tidal-mixing fronts in shelf seas, for instance in the Irish Sea (Hill, 1993) and in Georges Bank (Garrett et al., 1978; Loder, 1980; Loder and Wright, 1985; Naimie et al., 1994). The salinity, temperature and density structure in those frontal areas is similar to those in SPMB (Fig. 7) in the sense that the isoclines are spread vertically close to

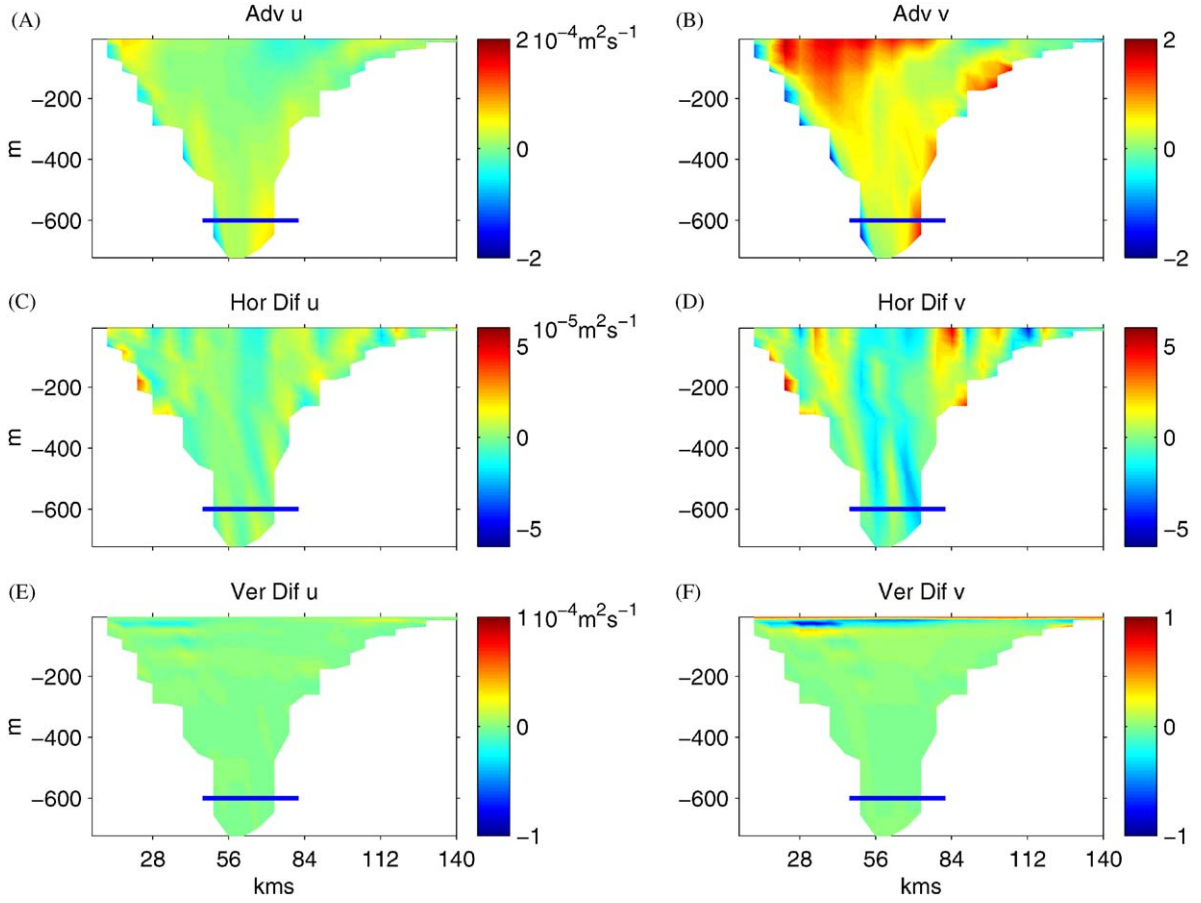

Fig. 9. Distribution on section "T" (looking up-gulf) of the time averaged terms of the momentum u ((A), (C), and (E)) and v ((B), (D), and (F)) equations: (A) and (B) advection, (C) and (D) horizontal diffusion, and (E) and (F) vertical diffusion. The horizontal thick lines show the position of the gyre.

the area where stirring is strong. Although in the Gulf stratification is not broken down to complete vertical homogeneity (Argote et al., 1995), mixing has profound consequences for the thermohaline structure, the circulation and the biological richness of the area (Alvarez-Borrego and Lara-Lara, 1991; Lavín and Marinone, 2003). Despite the obvious importance of mixing in the Gulf, there are no reported direct observations of the dissipation rate or generation of turbulent kinetic energy. Rather, parameterizations based on numerical models have been used, and we will do likewise here.

Energy transfer between different scales occurs through the nonlinear terms, viz. advection, friction against the bottom and internal mixing. In our model, we found all of these terms to be important in the area. As an example, Fig. 9 shows the time-averaged advection, horizontal and vertical diffusion terms of the momentum equations for the "T" section over SPMB (see Fig. 1). The Coriolis and pressure gradient terms, which are not shown, are equal or larger than those shown. Advection and vertical diffusion are larger than the horizontal diffusion term. The advective terms are largest on the West side (left of the figure), while vertical mixing is large in the upper part of the water column. Note that, when static instability is present in the model, the vertical eddy coefficient is assigned a maximum value of $0.2\,m^2/s$, until static stability is attained.

The capacity for mixing by the interaction of tidal currents with the bottom is proportional to the dissipation rate of tidal energy due to bottom friction, D_b (Argote et al., 1995):

$$D_b = C_{db}\,\rho T^{-1}\int^{T}(u^2+v^2)^{3/2}\,dt,$$

where (u,v) is the horizontal bottom velocity and T a period of time long enough to achieve a stable mean, ρ is density and $C_{db}=0.0037$. This term enters into the model in the vertical mixing term as a boundary condition (see Section 2.1). Fig. 10 shows this parameter integrated over a tidal period (M2) along the "T" section, calculated from the model outputs. Energy dissipation is largest in the deepest zone (40 km) just at the western edge of the gyre and in the East side (90–105 km) of the gyre, which is indicated in the figure as a horizontal line.

An important difference with the shelf seas is that in the Gulf of California tidal mixing occurs in the proximity of deep-water stratification (Simpson et al., 1994), so that in addition to bottom friction, internal mixing can be important (Marinone and Lavín, 2003; Filonov and Lavín, 2003), as also

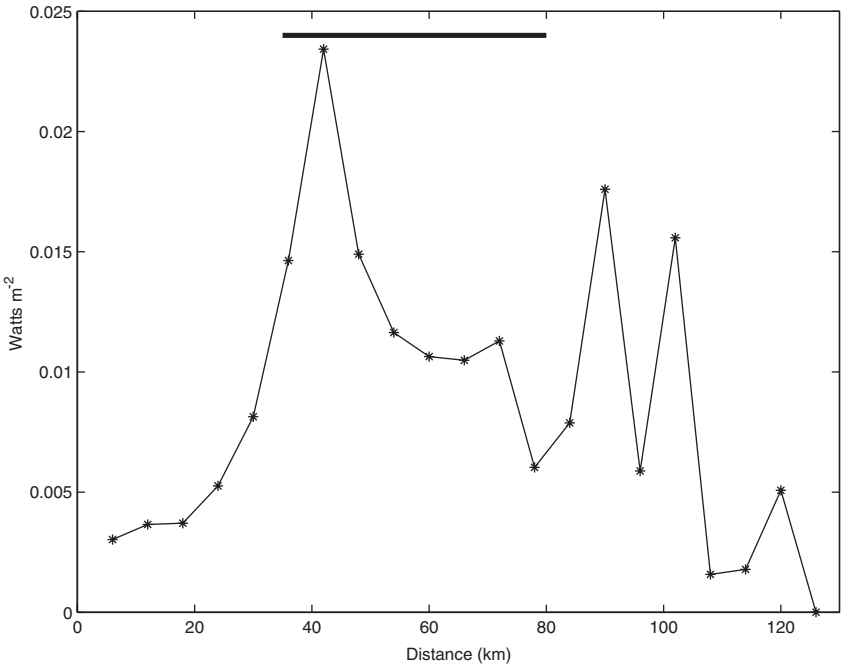

Fig. 10. Time-averaged dissipation energy rate (W/m) by bottom friction, on the "T" section in SPM Basin (the mainland is on the right-hand side). The horizontal line indicates the position of the SPBM gyre.

suggested by Fig. 9. A bulk measure of the degree of the internal mixing is the Froude number, defined as

$$Fr = \left[(\partial v/\partial z)^2/N^2\right]^{1/2} = Ri^{-1/2},$$

where $N^2 = (-g\rho^{-1}\,\partial\bar{\rho}/\partial z)$ is the Brunt–Vaisala frequency (see, e.g., Kundu,1990). For continuously stratified parallel flows, $Ri > \frac{1}{4}$ guarantees stability (Leblond and Mysak, 1978); thus, $Fr < 2$ is a sufficient condition for stability. A flow with $Fr > 2$ is not necessarily unstable, but very likely to become unstable, leading to turbulence and mixing.

In the surprising absence of detailed observational studies of turbulence and mixing in the Gulf of California, we have to resort to bulk estimates from our numerical model. Although the vertical scale over which these criteria were obtained is much smaller than the vertical resolution of our numerical model, it is useful to calculate *Fr*, at least as an indication of areas were relative *Fr* maxima are attained. Fig. 11 shows the distribution of *Fr* during the flood and the ebb, calculated from the model outputs, for the same times as Fig. 4. Although values of *Fr* are smaller than 2, there is some structure in the *Fr* field, suggesting that internal mixing processes may be occurring: (a) close to the bottom in the eastern side of the gyre and (b) in the thermocline in the central zone. West of the gyre, close to the peninsula coast, the *Fr* number is also large.

The model runs with and without tides demonstrate that the gyre is due mainly to the tides, and the density structure of both model and observations suggests that it is due to tidal mixing; but the specific mechanisms have not been discussed. Once again, in the absence of turbulence observations, indirect evidence must be used. A possible mechanism is the internal tide, which has been shown to be

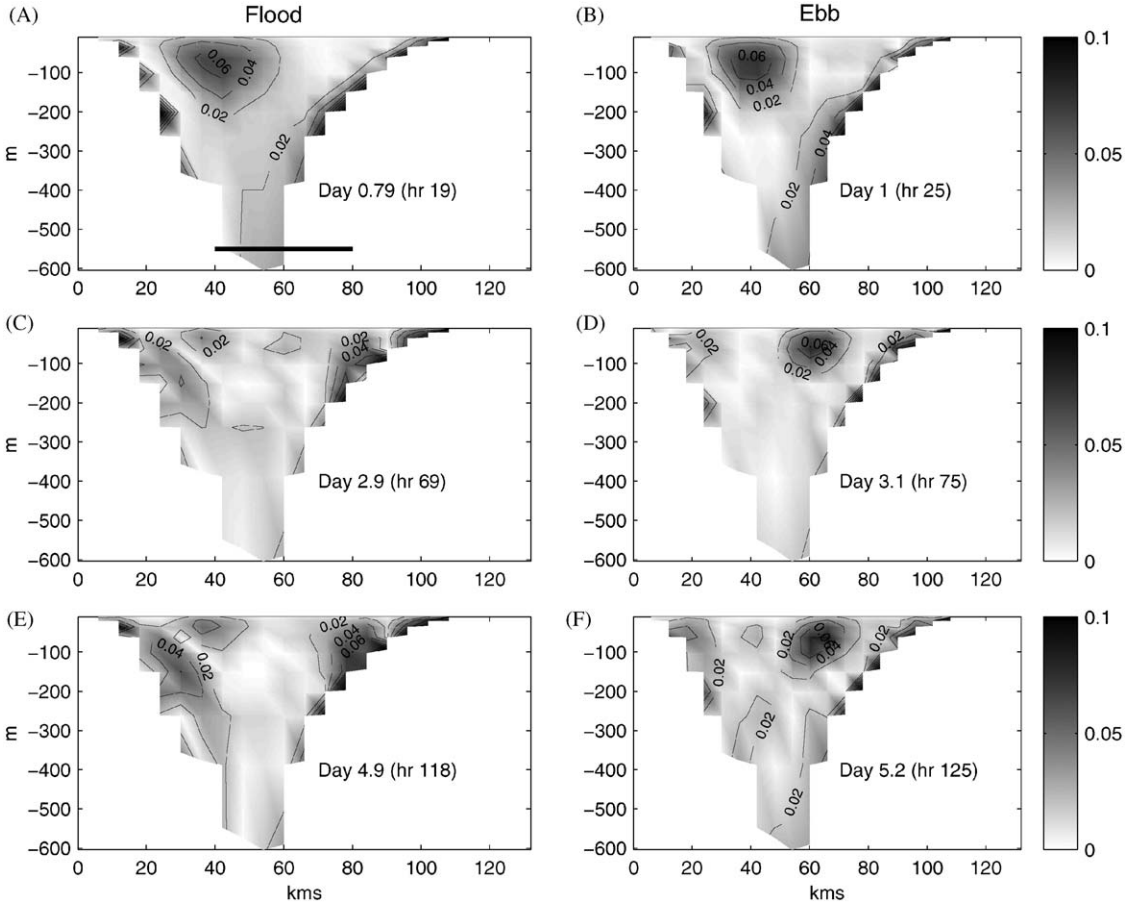

Fig. 11. Froude number evolution during flood and ebb on section "T" (looking up-gulf) for: (A) and (B) second day, (C) and (D) fourth day, (E) and (F) sixth day. The line in (A) marks the position of the gyre.

present in the area, caused by the interaction of the barotropic tide with steep bottom features in the presence of stratification (Marinone and Lavín, 2003; Filonov and Lavín, 2003). As a means of visualizing the internal tides, Fig. 12 shows the hourly evolution of $\partial v/\partial z$ (the vertical shear of the along-gulf velocity), which is related to the lateral density gradient through the thermal wind relation. Fig. 12 suggests the formation of mode one internal tides in the thermocline at ~50 km (western side of the gyre) and their propagation toward the coasts, where they may brake and dissipate producing mixing. The calculations were made from the M2 model run at a stage when the model was periodically stable; similar plots before 3–4 M2 cycles after the initiation of the run do not show internal tides.

Therefore, it seems that after forming the hydrographic structure that gives rise to the gyre very soon after the initiation of the model (as shown in Fig. 5), the barotropic tide maintains the structure by feeding energy for mixing through internal tides. Another possible source of internal mixing is the internal soliton packets reported by Fu and Holt (1984) and Badan-Dangon et al. (1991). Gaxiola-Castro et al. (2002) report that internal waves and tides have an effect on the Gulf of California phytoplankton, through pumping across the thermocline of nutrients and phytoplankton acclimatized to low light levels.

A conceptual model of the processes maintaining the gyre, and their respective zones of influence is sketched in Fig. 13. The top panel (Fig. 13A) shows the basin, the resultant shape of the isopycnals and the dynamic height of the surface. The bottom panel (Fig. 13B) shows distributions across the basin of smoothed versions of the time- and vertically averaged terms representing three different processes: bottom friction (compare this line with Fig. 10), internal mixing (vertical diffusion) and advection. The lines in the sketch are not comparable with one another, except for the advection and

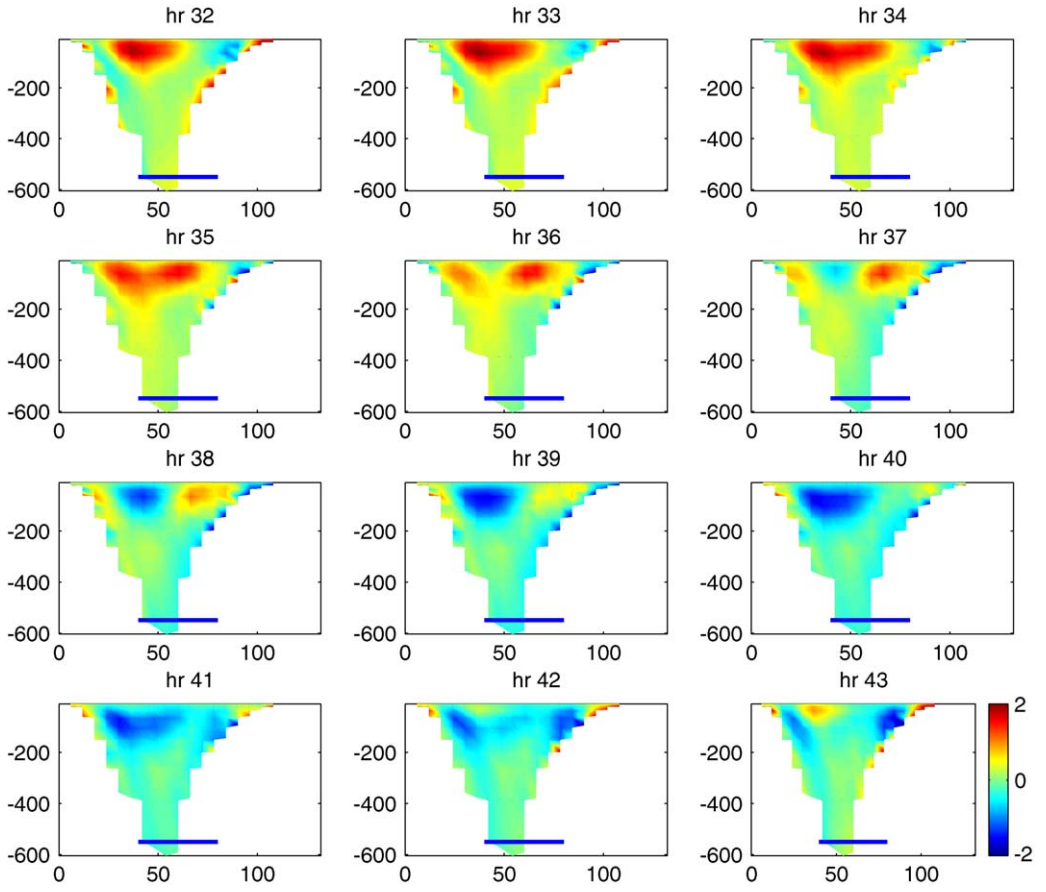

Fig. 12. Time series of the vertical shear of the along gulf velocity (in $10^{-3}\,s^{-1}$) on section "T" (looking up-gulf).

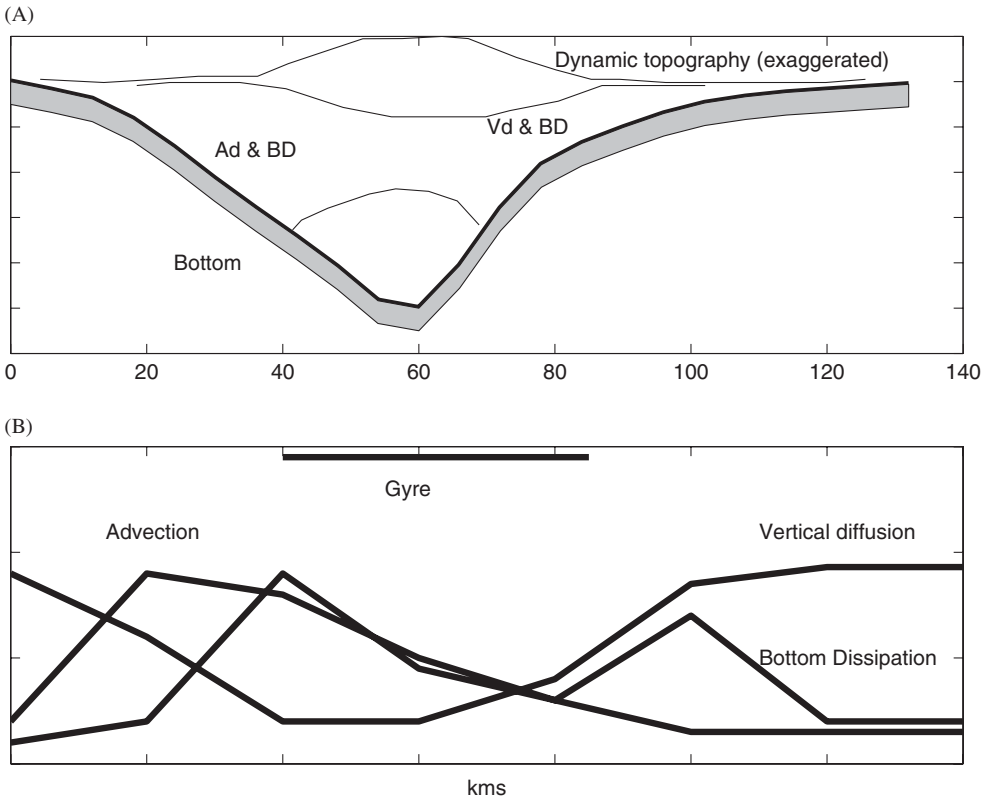

Fig. 13. (A) Sketch of the density structure and processes causing the anticyclonic gyre over SPMB; the mainland is on the right-hand side. Tidal mixing modifies the initially horizontal isopycnals, producing a dynamic height dome and therefore anticyclonic flow. (B) Sketch of the across-gulf distribution of processes leading to mixing (see text): the advection and vertical diffusion terms of the momentum equations, and the dissipation of tidal energy by bottom friction. On the East side of the gyre bottom dissipation (BD) and internal mixing (VD) occurs, while bottom dissipation (BD) and advection (Ad) are important on the West side.

vertical diffusion terms of the momentum equations; however, the relative importance for each individual process is suggested. In the East side of the gyre, mixing occurs due to both, boundary and internal mixing over the shelf. In the West side of the gyre, mixing and the transfer of energy to the water column are due to bottom dissipation and advection. The final consequence is the vertical spreading of the pycnocline to the sides of the gyre (Fig. 13A), giving rise to the anticyclonic gyre.

5. Conclusion

Evidence of the existence of the anticyclone gyre over SPMB, predicted by Marinone (2003) from a three-dimensional numerical model of the Gulf of California, was found in the geostrophic calculations and in the vertical profiles (S,T and ρ) from historical hydrographic data. The average distributions of temperature, salinity and density all show a concave shape over SPMB, which translates into a dynamic height dome and therefore into an anticyclonic gyre. Data from some individual cruises with good enough sampling showed the gyre, but most cruises sampling was poor, which forced the investigation to focus on the average conditions. More data, with higher sampling density over SPMB, are necessary to investigate more details and the seasonal cycle of the gyre; a cruise will soon be made to collect data with the specific purpose of further confirming the existence and describing the properties of the gyre.

The three-dimensional numerical-model investigation revealed that the tidal currents are responsible for the formation of the gyre; we propose that this occurs through vertical mixing and nonlinear interactions through bottom friction and advection, which are enhanced in SPMB due to the proximity of the sills and channels of the midriff archipelago where internal tides and soliton packets

are generated. The presence of stratification is also necessary, otherwise internal tides are not produced. Forcing by wind and the Pacific only alter the gyre in some months, and have no effect on the mean.

Considering the important role that mixing seems to play in many physical and biological features of the Gulf of California, the absence of turbulence studies is as surprising as potentially rewarding such studies would be.

Acknowledgments

This research was financed by CONACYT, through Grant 44055 of SGM and a scholarship to the first author, and CICESE's regular budget. MFL participation is part of CONACyT Contract D41881-F.

References

Alvarez-Borrego, S., Lara-Lara, R., 1991. The physical environment and primary productivity of the Gulf of California. In: Dauphin, J.P., Semmoneit, B.R. (Eds.), The Gulf of California and Peninsular Province of the Californias, Memoir 47. American Association of Petroleum Geologists, Tulsa, OK, pp. 555–567.

Argote, M.L., Amador, A., Lavín, M.F., Hunter, J.R., 1995. Tidal dissipation and stratification in the Gulf of California. Journal of Geophysical Research 100 (C8), 16103–16118.

Badan-Dangon, A., Koblinsky, C.J., Baumgartner, T., 1985. Spring and Summer in the Gulf of California observations of thermal patterns. Oceanologica Acta 8, 13–22.

Badan-Dangon, A., Hendershott, M.C., Lavín, M.F., 1991. Underway Doppler current profiles in the Gulf of California. Eos Transactions American Geophysical Union 72 pp. 209, 217–218.

Figueroa, J.M., Marinone, S.G., Lavín, M.F., 2003. A description of geostrophic gyres in the southern Gulf of California. In: Velasco Fuentes, O.U., Sheinbaum, J., Ochoa, J. (Eds.), Nonlinear Processes in Geophysical Fluid Dynamics. Kluwer Academic Publishers, Dordrecht, pp. 237–255.

Filloux, J.H., 1973. Tidal patterns and energy balance in the Gulf of California. Nature 243, 217–221.

Filonov, A.E., Lavín, M.F., 2003. Internal tides in the northern Gulf of California. Journal of Geophysical Research 108 (C5), 3151 doi:10.1029/2002JC001460.

Fomin, L.M., 1984. Calculation of the absolute velocity of currents in the ocean by the dynamic method, based on the principle of minimum of kinetic energy. Oceanology 24, 33–39.

Fu, L.L., Holt, B., 1984. Internal waves in the Gulf of California: observations from a spaceborn radar. Journal of Geophysical Research 89, 11765–11778.

Garrett, C.J.R., Keeley, J.R., Greenberg, D.A., 1978. Tidal mixing versus thermal stratification in the Bay of Fundy and Gulf of Maine. Atmosphere Ocean 16 (4), 403–423.

Gaxiola-Castro, G., Alvarez-Borrego, S., Nájera-Martínez, S., Zirino, A.R., 2002. Internal waves effect on the Gulf of California phytoplankton. Ciencias Marinas 28, 297–309.

Hendershott, M.C., Speranza, A., 1971. Co-oscillating tides in long narrow bays: the Taylor problem revisited. Deep Sea Research 18, 959–980.

Hill, A.E., 1993. Seasonal gyres in shelf seas. Annual Geophysicae 11, 1130–1137.

Kochergin, V.P., 1987. Three-dimensional prognostic models. In: Heaps, N.S. (Ed.), Three-Dimensional Coastal Ocean Models. American Geophysical Union, Washington, DC.

Kundu, P.K., 1990. Fluid Mechanics. Academic Press, NY, 538pp.

Lavín, M.F., Marinone, S.G., 2003. An overview of the physical oceanography of the Gulf of California. In: Velasco Fuentes, O.U., Sheinbaum, J., Ochoa, J. (Eds.), Nonlinear Processes in Geophysical Fluid Dynamics. Kluwer Academic Publishers, Dordrecht, pp. 173–204.

Lavín, M.F., Durazo, R., Palacios, E., Argote, M.L., Carrillo, L., 1997. Lagrangian observations of the circulation in the northern Gulf of California. Journal of Physical Oceanography 27, 2298–2305.

LeBlond, P.H., Mysak, L.A., 1978. Waves in the Ocean. Elsevier Oceanographic Series.

Loder, J.W., 1980. Topographic rectification of tidal currents on the sides of Georges Banks. Journal of Physical Oceanography 10, 1399–1416.

Loder, J.W., Wright, D.G., 1985. Tidal rectification and frontal circulations on sides of Georges Bank. Journal of Marine Research 43, 581–604.

Marinone, S.G., 2003. A three dimensional model of the mean and seasonal circulation of the Gulf of California. Journal of Geophysical Research 108 (C10), 3325 doi:10.1029/2002JC001720.

Marinone, S.G., Lavín, M.F., 2003. Residual flow and mixing in the large islands region of the central Gulf of California. In: Velasco Fuentes, O.U., Sheinbaum, J., Ochoa, J. (Eds.), Nonlinear Processes in Geophysical Fluid Dynamics. Kluwer Academic Publishers, Dordrecht, pp. 213–236.

Marinone, S.G., Lavín, M.F., 2005. Tidal current ellipses in a three-dimensional baroclinic numerical model of the Gulf of California. Estuarine, Coastal and Shelf Sciences 64, 519–530.

Marinone, S.G., Ripa, P., 1988. Geostrophic flow in the Guaymas Basin, central Gulf of California. Continental Shelf Research 8 (2), 159–166.

Naimie, C.E., Loder, J.W., Lynch, D.R., 1994. Seasonal variation of the three-dimensional residual circulation on Georges Bank. Journal of Geophysical Research 99, 15967–15989.

Navarro-Olache, L.F., Lavín, M.F., Alvarez Sánchez, L.G., Zirino, A., 2004. Internal structure of SST features in the central Gulf of California. Deep Sea Research Part II 51, 673–687.

Paden, C.A., Abbott, M.R., Winant, C.D., 1991. Tidal and atmospheric forcing of the upper ocean in the Gulf of California 1. Sea surface temperature variability. Journal of Geophysical Research 96, 18337–18359.

Pegau, W.S., Boss, E., Martínez, A., 2002. Ocean color observations of eddies during the summer in the Gulf of

California. Geophysical Research Letters 29 (9) 10.1029/2001GL014076.

Pond, S., Pickard, G., 1983. Introductory Dynamical Oceanography. Pergamon Press, Oxford 241pp.

Simpson, J.H., 1981. The Shelf-sea fronts: implications of their existence and behavior. Philosophical Transactions of the Royal Society of London 302, 531–546.

Simpson, J.H., Souza, A.J., Lavín, M.F., 1994. Tidal mixing in the Gulf of California. In: Beven, K.J., Chatwin, P.C., Millbank, J.H. (Eds.), Mixing and Transport in the Environment. Wiley, New York, pp. 169–182.

Takeoka, H., Kaneda, A., Anami, H., 1997. Tidal Fronts induced by horizontal contrast of vertical mixing efficiency. Journal of Oceanography 53, 563–570.